Models for Ferredoxins: Electronic Structures of Iron-Sulfur Clusters with One, Two, and Four Iron Atoms

Louis Noodleman,*[1a,b] Joe G. Norman, Jr.,[1a] Joseph H. Osborne,[1c] Arie Aizman,[1d] and David A. Case*[1e]

Contribution from the Department of Chemistry, University of Washington, Seattle, Washington 98195, Depto. de Quimica, Facultad de Ciencias Basicas y Farmaceuticas, Universidad de Chile, Santiago, Chile, and Department of Chemistry, University of California, Davis, California 95616. *Received October 25, 1984*

Abstract: We report results of Xα valence bond scattered wave (Xα-VB-SW) calculations for a variety of clusters that mimic the active sites in iron-sulfur proteins: $Fe(SR)_4^{1-,2-}$ (R = H, CH_3), $Fe_2S_2(SH)_4^{2-,3-}$, and $Fe_4S_4(SCH_3)_4^{2-,3-}$. Emphasis is placed on comparisons among the various clusters, including changes in the elctron distribution upon reduction, upon going from low spin to high spin, and upon changes in cluster geometry. We present estimates based on the calculations of Mössbauer isomer shifts and quadrupole splittings which lead to a consistent account of many experimental observations. The calculations predict the iron-(bridging sulfur) bonds to be stronger than those between iron and the terminal sulfur atoms; this has interesting structural and spectroscopic implications. To a good approximation, the oxidized 4-Fe complex can be viewed as two high-spin reduced 2-Fe clusters, despite the differences in geometry. Some of the implications of these results for structure-function problems in iron-sulfur proteins are discussed.

Iron-sulfur proteins are widely distributed in both lower and higher organisms. Most of the proteins characterized so far contain iron-sulfur clusters with one, two, or four iron atoms, connected to the protein through the side chains of cysteine amino acids, as shown in Figure 1. Many of these clusters serve as the active sites for electron transport, but a variety of other catalytic functions have also been proposed.[2] Quantum mechanical descriptions of the electronic structures of such complexes should aid interpretation of the magnetic properties, spectroscopy, and, ultimately, the chemistry of these species. However, the problem of obtaining useful wave functions is not an easy one, because of the large number of electrons and the relatively weak interactions between the transition metals.

Recent theoretical calculations on active site models for 2-Fe and 4-Fe iron-sulfur proteins have emphasized the importance of a valence-bond (VB)-like description of the iron sites and their interactions. In its simplest form, this corresponds to the spin Hamiltonian commonly used to interpret Mössbauer and magnetic resonance spectra, in which each iron atom is assigned a spin of $^5/_2$ or 2, and these sites interact through ferromagnetic or antiferromagnetic coupling.[3] A more correct model must include delocalization of the charge and spin densities onto the ligands.

One approach to such a description is through spin-unrestricted broken symmetry molecular orbital (MO) calculations. This technique can interpolate between the conventional VB and MO limits, yielding an energy lower than either, with a wave function that gives a qualitatively correct picture of antiferromagnetic coupling between the largely localized spins on each iron site. Calculations of this type have been reported for oxidized 2-Fe and 4-Fe clusters (using the Xα scattered wave technique[4,5]) and for both oxidized and reduced 2-Fe clusters (using an Xα basis set expansion method.[6]).

Here we present in detail Xα scattered wave results for reduced forms of the 2-Fe and 4-Fe clusters, and extend previous results[7] for the 1-Fe clusters found in rubredoxin. This gives, for the first time, a set of calculations for all of these species at a common level of theory. We use these results to compute the charge and spin distributions as a function of cluster size and overall oxidation state, and for ferromagnetic vs. antiferromagnetic coupling schemes. In addition, we compare calculated and experimental Mössbauer isomer shifts and quadrupole splittings, showing that the qualitative features of these measurements can be understood in terms of the broken symmetry orbital picture.

The present results also extend previous calculations by considering possible geometrical variations in the 2-Fe and 4-Fe clusters. For the 2-Fe clusters, the orientation of the S-H bond directions relative to the cluster "core" is connected in an important way to the Mössbauer quadrupole splittings, the g tensors, and the predicted excitation energies. For the 4-Fe clusters, tetragonal distortions that both compress and elongate the core along an S_4 axis are considered. Although we are not able at present to determine theoretically optimized geometries, these results give some measure of the sensitivity of the charge and spin distributions to changes in geometry.

In a separate paper, we compare the results of these scattered wave calculations to Hartree-Fock-based configuration interaction calculations (for the 1-Fe cluster) and to basis set Xα calculations (for the 2-Fe clusters).[8] These complement earlier comparisons of scattered wave and basis set Xα calculations for the 4-Fe clusters.[5] In general, the comparisons show that the approximations involved in multiple scattering theory are not severe for these fairly compact clusters. In particular, all of the trends in charge and spin distributions reported below for the 2-Fe clusters are also seen in the basis set calculations, although actual values predicted by the two methods are somewhat different.[8] There are some significant differences between the predictions of scattered wave and basis set calculations for the energies of charge-transfer excited states, but the differences in the ground-state properties are minor. It is only for the scattered wave calculations that we have available results for the whole range of clusters at a common level of approximation, and we use the trends predicted by the calculations to study their common features.

(1) (a) University of Washington. (b) Current address: Center for Bioengineering, WD-12, University of Washington, Seattle, WA 98195. (c) Current address: Department of Chemistry, University of California, San Diego. (d) Universidad de Chile, to whom correspondence in the southern hemisphere should be addressed. (e) University of California, Davis.

(2) (a) Lovenberg, W. Ed.; "Iron-Sulfur Proteins"; Academic Press: New York, 1973; Vol. I and II; 1977, Vol. III. (b) Sweeney, W. V.; Rabinowitz, J. C. *Annu. Rev. Biochem.* **1980**, *49*, 139. (c) Spiro, T. G., Ed.; "Iron-Sulfur Proteins", Academic Press: New York, 1981.

(3) See, e.g.: Gibson, J. F.; Hall, D. D.; Thornley, J. H.; Whatley, F. R. *Proc. Natl. Acad. Sci. U.S.A.* **1966**, *56*, 987. Cammack, R.; Dickson, D. P. E.; Johnson, C. E. In ref 2a, Vol. III, pp 283-300.

(4) Norman, J. G., Jr.; Ryan, P. B.; Noodleman, L. J. *J. Am. Chem. Soc.* **1980**, *102*, 4279.

(5) Aizman, A.; Case, D. A. *J. Am. Chem. Soc.* **1982**, *104*, 3269.

(6) Noodleman, L.; Baerends, E. J. *J. Am. Am. Chem. Soc.* **1984**, *106*, 2316.

(7) Norman, J. G., Jr.; Jackels, S. C. *J. Am. Chem. Soc.* **1975**, *97*, 3833.

(8) Noodleman, L.; Norman, J. G., Jr.; Osborne, J.; Case, D. A., manuscript in preparation.

0002-7863/85/1507-3418$01.50/0

Table I. Geometries Used in the Calculations[a]

cluster:	$Fe(SCH_3)_4$	$Fe_2S_2(SH)_4$		$Fe_4S_4(SCH_3)_4$	
charge:	1-, 2-	2-	3-	2-	3-
geometry:		A, B	C, D	E	F
		A. Bond Lengths[b]			
Fe-S	2.29	2.31	2.31, 2.38	2.25	2.30
Fe-S*		2.21	2.21, 2.28	2.24 (4), 2.31 (8)	2.35 (4), 2.29 (8)
Fe-Fe		2.69	2.73	2.73 (4), 2.78 (2)	2.74
		B. Bond Angles[c]			
Fe-S*-Fe		75.0	75.0	73.8	72.9
S-Fe-S	109.5	109.5	109.5		
S*-Fe-S*		105.0	107.3, 102.7	104.1	104.8
Fe-S-R	107.2	109.5	109.5	103.0	103.0

[a] The S-H bonds point toward the Fe-Fe axis in geometries A and C, and away from it in geometries B and D; see text. [b] In Å. [c] In degrees.

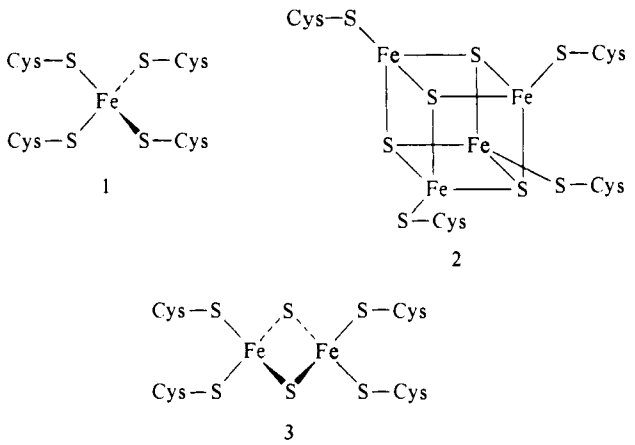

Figure 1. Types of iron-sulfur clusters considered in this paper.

Computational Section

The scattered wave calculations reported here are analogous to those of earlier papers,[4,5,7] so that only those features unique to the present work are presented here. The Xα multiple scattering method has been reviewed recently,[9] and computer codes are available from the Quantum Chemistry Program Exchange[10] and the National Energy Software Center.[11]

The geometries used in the present calculations are collected in Table I. Generally, the structures chosen for the theoretical models have some dimensions averaged to retain elements of molecular symmetry.

For the 2-Fe clusters, two values of the S*-Fe-S-H torsion angle are considered. (Here S* represents the bridging or "inorganic" sulfur). These are labeled "A" and "B" for the oxidized cluster, and "C" and "D" for the reduced cluster. The S-H bonds in structures "A" and "C" point toward the Fe-Fe (z) axis, rather than away from it, as in structures "B" and "D". In all cases the entire $Fe(SH)_2$ unit is coplanar. For the oxidized structures, the two halves of the molecule are identical, and the overall symmetry is D_{2h}. The reduced model geometries differ from the oxidized form by a 0.07 Å increase in all Fe-S bonds at the reduced site; the overall symmetry is thus C_{2v}. Hence our reduced structures correspond to a trapped valuence situation in which the iron(II) and iron(III) sites see different local geometries. Earlier calculations have shown that a trapped valence picture is appropriate even in a D_{2h} geometry,[6] and experimental results for proteins and model compounds with reduced 2-Fe clusters are in accord with this notion.[12,13]

For the 4-Fe clusters, a variety of distortions from idealized tetrahedral core symmetry are seen experimentally in model compounds and in proteins.[14,15] The model structures that most closely correspond to those in proteins can be viewed as involving a tetragonal distortion along an S_4 axis of the core. In the oxidized clusters, a compression occurs, yielding four "short" and eight "long" Fe-S* distances. Such a geometry ("E" in Table I) was used in our earlier calculations on oxidized 4-Fe clusters,[5] and is based on the idealized structure[14] of the tetraethylammonium salt of $Fe_4S_4(SCH_2Ph)_4^{2-}$. In the reduced species, there appears to be a general expansion of the core, sometimes accompanied by a tetragonal elongation, leading to four "long" and eight "short" Fe-S* distances. Our idealized structure is labeled "F" in Table I and is based on that of $Fe_4S_4(SPh)_4^{3-}$, which also has approximate D_{2d} geometry.[15] Calculations on the reduced species are reported here for both geometries "E" and "F".

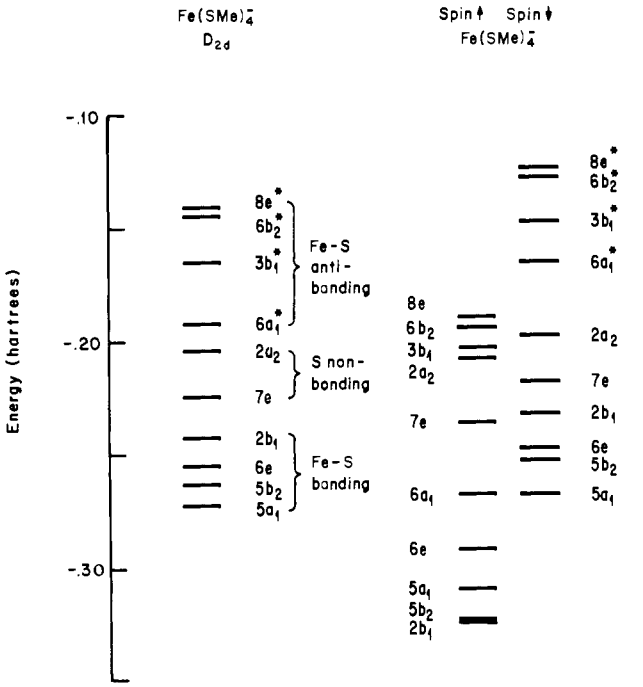

Figure 2. SCF-Xα-SW-MO energy levels for the oxidized rubredoxin model $Fe(SCH_3)_4^-$ above -0.33 hartree, in D_{2d} symmetry. All levels are fully occupied except those marked with an asterisk, which are half-filled in the spin-restricted diagram and empty in the spin-polarized diagram. Valence energy levels below -0.33 hartree are largely localized on the CH_3S^- ligand (see ref 7): 1 hartree = 27.2 eV.

Other details of the calculations, including sphere radii and α parameters, are given in previous papers.[4,5,7] All calculations were carried out in double precision (64-bit arithmetic) on IBM 4041 or DEC VAX 11/780 machines, or in single precision (60-bit arithmetic) on CDC 7600 or CYBER 170/750 machines.

Molecular Orbital Energies

Broken symmetry molecular orbital energy diagrams for one-, two-, and four-iron clusters are presented in Figures 2-4. These

(9) Case, D. A. *Annu. Rev. Phys. Chem.* **1982**, *33*, 151.
(10) Program No. 465, Bloomington, Ind.
(11) Argonne National Laboratory, Argonne, IL 60439, Acquisition No. 961.
(12) Sands, R. H.; Dunham, W. R. *Q. Rev. Biophys.* **1975**, *4*, 443.
(13) Mascharak, P. K.; Papaefthymiou, G. C.; Frankel, R. B.; Holm, R. H. *J. Am. Chem. Soc.* **1981**, *103*, 6110.
(14) Averill, B. A.; Herskovitz, T.; Holm, R. H.; Ibers, J. A. *J. Am. Chem. Soc.* **1973**, *95*, 3523. See also: Mascharak, P. K.; Hagen, K. S.; Spence, J. T.; Holm, R. H. *Inorg. Chim. Acta* **1983**, *80*, 157.
(15) (a) Berg, J. M.; Hodgson, K. O.; Holm, R. H. *J. Am. Chem. Soc.* **1979**, *101*, 4586. (b) Laskowski, E. J.; Frankel, R. B.; Gillum, W. O., Papaefthymiou, G. C.; Renand, J.; Ibergs, J. A.; Holm, R. H. *Ibid.* **1978**, *100*, 5322. (c) Stephan, D. W.; Papaefthymiou, G. C.; Frankel, R. B., Holm, R. H. *Inorg. Chem.* **1983**, *22*, 1550.

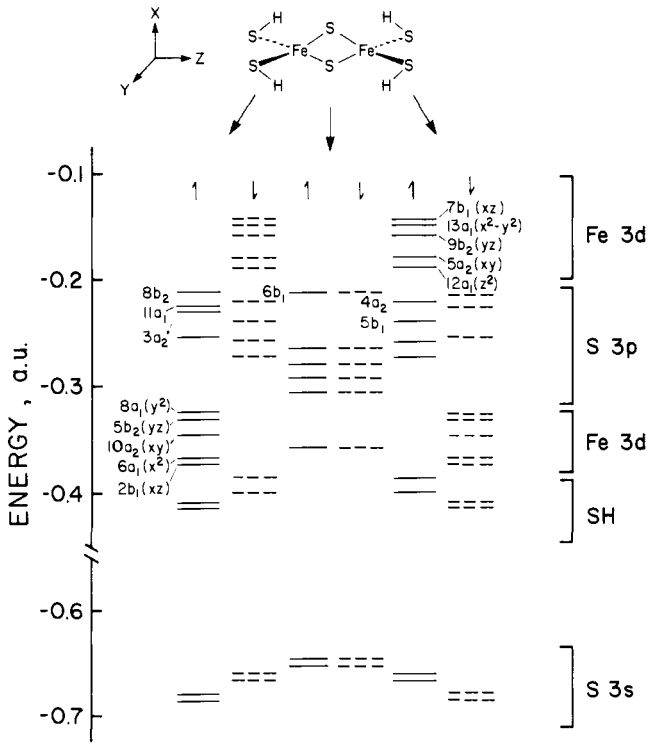

Figure 3. Orbital energy diagram for $Fe_2S_2(SH)_4^{2-}$ in geometry D. Orbitals on the left, center, and right side of the diagram are approximately localized on the corresponding region of the molecule. An analogous figure for geometry C is given in ref 4. Basis set Xα results for geometry D may be found in ref 6: 1 hartree = 27.2 eV.

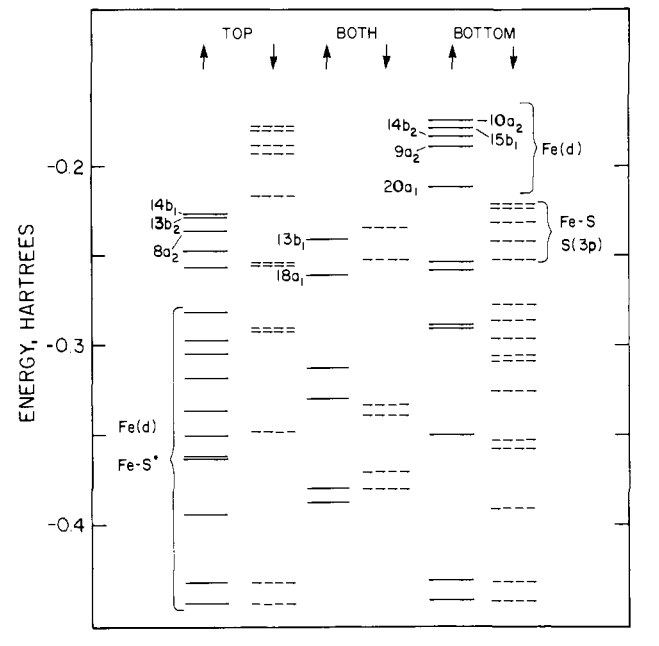

Figure 4. Orbital energy diagram for $Fe_4S_4(SCH_3)_4^{3-}$ in geometry F. Localization at the top or bottom of the molecule, as shown in Figure 1, is indicated. An analogous figure for the 2- oxidation state is given in ref 5: 1 hartree = 27.2 eV.

were determined by a "spin-unrestricted" procedure, which allows different orbitals for different spins. In addition, for the two- and four-iron cases, a "broken symmetry" procedure was used, in which the symmetries of the orbitals (C_{2v}) are allowed to be lower than that of the nuclear framework (which is D_{2h} or D_{2d}). This symmetry lowering removes the reflection plane through the two S* atoms (for the 2-Fe cluster) or the S_4 operation that interconverts the "top" and "bottom" of the molecule (for the 4-Fe cluster). The orbitals may then partially localize on one side of the molecule or the other, yielding orbitals similar to those that would be found

Table II. Orbital Energies and Charges for $[Fe_4S_4(SCH_3)_4]^{2-,3-}$

		charge distribution[b]					
		Fe		S		S*	
orbital[a]	energy, eV	top	bottom	top	bottom	top	bottom
$14b_2$	-6.17	4	82	1	1	11	1
	4.97	3	87	0	1	8	1
	-5.27	3	88	0	1	7	0
$9a_2$[c]	-6.24	3	72	0	13	9	2
	-5.10	3	80	0	9	7	1
	-5.39	3	82	0	9	5	1
$20a_1$[d]	-6.89	2	87	2	3	1	4
	-5.71	1	92	1	2	0	3
	-5.95	1	93	0	2	0	4
$13b_2$	-7.07	21	10	49	1	15	4
	-6.23	28	8	38	1	22	0
	-6.35	33	8	33	1	25	0
$14b_1$	-7.08	32	15	26	1	20	4
	-6.19	35	12	26	0	23	3
	-6.28	35	10	30	0	22	2
$8a_2$	-7.20	10	2	77	0	5	0
	-6.45	12	2	74	0	7	0
	-6.59	13	2	77	0	7	0

[a] All orbitals shown are spin α. For each orbital, the top line refers to the 2- calculation; the middle line is for the 3- cluster in the 2- ("E") geometry; the bottom line is for the 3- cluster in the expanded ("F") geometry. [b] Charges, in percent of one electron. Top and bottom refer to top and bottom of the cluster as in Figure 1. [c] Highest occupied orbital in the 3- cluster. [d] Highest occupied orbital in the 2- cluster.

in a generalized valence bond calculation. For this reason, the method has been called the Xα-VB approach.[4,16]

It is important to realize that the single determinant wave function calculated in this fashion has neither the space nor spin symmetry expected for the true wave function. Spatial symmetry can be imposed by adding the "mirror image" (or "S_4 image"[5]) wave function, and we will always take the resulting two-determinant wave function as our model solution. Approximate spin projection techniques may then be used to obtain estimates of the energies of the true spin states of the cluster.[16,17] Such projections enable one to calculate antiferromagnetic coupling constants, but they are not required for the conclusions reported here, which are obtained from the *qualitative* features of the broken symmetry molecular orbital model. A detailed discussion of the connection between the broken symmetry model and other approximate wave functions is given elsewhere.[6,17]

Several common features are evident in the molecular orbital energy diagrams. In all cases five occupied Fe 3d-like orbitals (the ones occupied in the formal +3 oxidation state) are found well down in the valence band, below occupied orbitals which are mainly sulfur 3p in character. Higher yet are the orbitals made up primarily from the remaining five iron 3d orbitals; some of these will be occupied if the average formal oxidation state is less than +3. This simple classification scheme is useful, but it must be remembered that all of the orbitals are delocalized to some extent; the "iron" orbitals identified above, for example, contain 10–30% sulfur character as well.

Figures 2, 3, and 4 show results for the "oxidized" one- and two-iron clusters, and for the "reduced" form of the four-iron cluster. In general, the differences between the oxidized and reduced diagrams for a given cluster levels are minor, indicating that the presence of an extra electron has only a small effect on the orbital energies, aside from a uniform upward shift. In the even-electron, oxidized clusters there is a "mirror symmetry" in the molecular orbitals such that a spin-up orbital on the left has a partner of equal energy which is spin-down and on the right (see, e.g., Figure 3). This symmetry is broken slightly in the odd-electron reduced clusters, but as seen in Figure 4, for the most part each orbital still has a partner, although one with a slightly different energy.

(16) Noodleman, L.; Norman, J. G., Jr. *J. Chem. Phys.* **1979**, *70*, 4903.
(17) Noodleman, L. *J. Chem. Phys.* **1981**, *74*, 5737.

Table III. Ground-State Charge and Spin Populations[a]

	$Fe(SCH_3)_4$		$Fe_2S_2(SH)_4$		$Fe_4S_4(SCH_3)_4$	
cluster charge:	−1	−2	−2	−3	−2	−3
formal Fe oxidation state:	+3	+2	+3	+3, +2	+2.5	+2.5, +2
			A. Valence Populations			
Fe (3d)	6.57	6.88	6.80	6.80, 7.02[b]	6.95	6.99, 7.05[b]
Fe (total)	8.05	8.38	8.02	8.07, 8.13	8.05	8.07, 8.12
S*			6.42	6.57	6.27	6.37, 6.35
S	6.20	6.34	6.35	6.43, 6.53	6.18	6.28, 6.31
			B. Spin Populations[c]			
Fe (3d)	+3.43	+3.12	±2.84	+2.98, −2.65	±2.77	+2.85, −2.60
Fe (total)	+3.64	+3.30	±3.00	+3.13, −2.74	±2.92	+2.97, −2.71
S*			0	+0.13	±0.06	+0.17, −0.04
S	+0.24	+0.10	±0.27	+0.24, −0.15	±0.39	+0.27, −0.18

[a] Cluster geometries are given in Table I. For $Fe_2S_2(SH)_4^{3-}$, geometry D was used; for $Fe_4S_4(SCH_3)_4^{3-}$ geometry F. Values for the 2-Fe and 4-Fe complexes are for the low-spin (antiferromagnetic) forms. [b] First value refers to the more highly oxidized half of the molecule, the second value to the more highly reduced half. [c] Positive sign indicates excess of spin-up electrons.

This similarity between oxidized and reduced complexes is true for orbital populations as well as energies. To illustrate this, we report in Table II the charge distribution of orbitals near the Fermi level for the 4-Fe cluster. For each orbital, comparison of the top two lines shows the effect of adding an electron with no change in geometry, while a comparison of the second and third lines shows the sensitivity of the reduced cluster to a change in geometry. Although the changes are small, the general trend upon reduction is to increase the localization of orbitals, i.e., orbitals such as $20a_1$, $9a_2$, and $14b_2$, which are localized on the bottom irons in the 2− complex, are more strongly localized in the 3− complex. The expansion of the core that takes place in going from geometry E to F also increases this localization. In terms of the molecular orbital distributions, then, the reduced complexes appear to be slightly closer to the localized valence bond limit than are the oxidized complexes, but the differences are not great.

In spite of these similarities in orbital energies and characters, the overall electronic changes upon reduction cannot be understood in terms of just the accepting orbital, because the small changes that do take place in many of the other valence orbitals have an important cumulative effect. We examine this behavior in the next section.

The oxidized 4-Fe complex can be considered formally to arise from the antiferromagnetic coupling of two high-spin reduced 2-Fe subunits, each having $S = {}^9/_2$.[18] Our energy level diagrams support such a model. A diagram for the high-spin 2-Fe complex is shown in Figure 5; these may be compared with results for the low-spin 4-Fe complex shown in Figure 4. For both complexes the highest occupied molecular orbital is mainly a symmetric combination of Fe $3d_{z^2}$ orbitals (with respect to a local Fe–Fe z axis); this orbital also has some contribution from $3d_{x^2-y^2}$, as discussed below. The first two spin-down LUMO's of the reduced 2-Fe cluster (3− ion) are of a_u and b_{1u} symmetry, and closely resemble the $9a_2$ and $14b_2$ LUMO's of $Fe_4S_4(SCH_3)_4^{2-}$. Using a local z axis along the Fe–Fe direction, and letting the xz plane be the mean plane of the top of the 4-Fe "cube", these orbitals mainly have the form $(d_{xy})_{left}-(d_{xy})_{right}$ for a_u and $9a_2$, and $(d_{z^2})_{left}-(d_{z^2})_{right}$ for b_{1u} and $14b_2$. In an earlier paper[6] we showed that *high-spin* reduced 2-Fe clusters are expected to have a delocalized structure (as shown in Figure 5), in contrast to the trapped valence situation expected for the *low-spin* 2-Fe clusters. This is consistent with our model of the 4-Fe clusters being made up of delocalized, high-spin 2-Fe clusters, and with Mössbauer evidence that fails to find spin trapping in the 4-Fe clusters.

Charge and Spin Distributions

Table III compares the charge and spin populations for ground states of the one-, two-, and four-iron clusters. It is useful to compare these values with those of idealized structures. In the localized VB (or spin Hamiltonian) model, the oxidized one- and two-iron clusters have iron atoms that are formally in the +3 state. This model predicts a charge of +3 electrons and a spin population (spin-up minus spin-down) of +5. The other clusters have smaller formal charges on iron, as shown in Table III. In the delocalized (restricted) MO model the spin populations become zero for the diamagnetic states, and the charges are the same for each symmetry-equivalent iron atom.

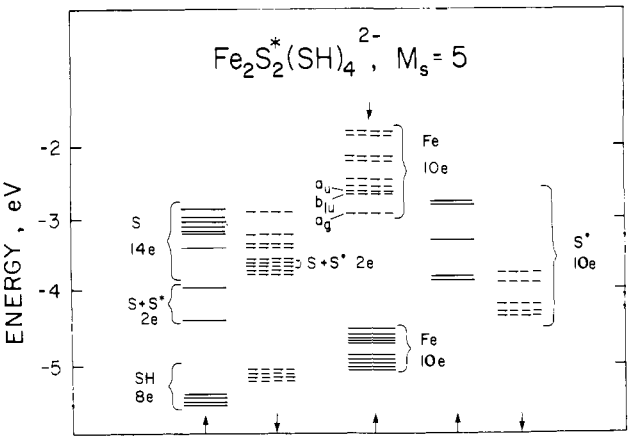

Figure 5. Orbital energy diagram for the high-spin form of $Fe_2S_2(SH)_4^{2-}$. Localization information is only approximate, since all orbitals are delocalized. In the 2− form, the LUMO is a_g; for 3−, a_g is the HOMO, and b_{1u} is LUMO with a_u nearby.

Covalent bonding with the ligands substantially reduces the net charge on the iron atoms, so that they have ${}^1/_2$–7 d electrons, and a neutral or slightly negative total charge. The largest spin population is +3.6 for the oxidized 1-Fe cluster. There are also substantial spin populations at the sulfur sites, with the bridging sulfur having smaller values than the terminal sulfurs; the bridging positions are also slightly more negative in total charge than the terminal ones. Hence all of the clusters are intermediate between the delocalized MO limit (for which all spin populations are zero) and the localized VB limit (in which the spin is localized at the iron sites.)

The 1-Fe clusters have smaller d-orbital occupations and higher spin densities at iron than the larger clusters in equivalent formal oxidation states. This suggests that Mössbauer and ESR parameters found for rubredoxins may be only partially transferrable to multinuclear clusters. On the other hand, the 2-Fe and 4-Fe clusters are much more nearly alike in their charge and spin populations; we explore this comparison in more detail below.

Table IV gives results for the *high-spin* or ferromagnetic forms of the 2-Fe and 4-Fe complexes. These correspond to molecular excited states in which the spin directions for the two halves of the molecule are parallel, rather than being antiparallel as in the low-spin ground states. Breaking symmetry does not lower the total energy in this case, so that these results correspond to

(18) Dickson, D. P. E.; Johnson, C. E.; Thompson, C. L.; Cammack, R.; Evans, M. C. W.; Hall, D. O.; Rao, K. K.; Weser, U. *J. Phys. (Paris)* **1974**, *35*, C6-343. See also ref 3.

Table IV. Charge and Spin Populations for High-Spin Clusters[a]

	$Fe_2S_2(SH)_4$		$Fe_4S_4(SCH_3)_4$	
net charge:	−2	−3	−2	−3
formal Fe charge:	+3	+2.5	+2.5	+2.25
	A. Valence Populations			
Fe (3d)	6.73	6.85, 6.87	6.87	6.94
Fe (total)	7.98	8.14, 8.00	7.98	8.03
S*	6.49	6.65	6.35	6.44
S	6.33	6.45, 6.47	6.17	6.28
	B. Spin Populations			
Fe (3d)	+3.14	+3.04, +3.03	+3.15	+3.12
Fe (total)	+3.29	+3.19, +3.15	+3.32	+3.25
S*	+0.58	+0.45	+0.61	+0.56
S	+0.33	+0.24, +0.22	+0.49	+0.40

[a] See footnotes to Table III.

conventional, spin-unrestricted MO calculations. (However, in the reduced form of the 2-Fe complex, the iron–sulfur bond lengths are different in the two halves of the molecule, as shown in Table I, leading to slightly inequivalent populations.) Compared to the low-spin forms, the high-spin complexes have lower d-orbital occupations and higher spin populations. This makes the multinuclear high-spin complexes more like the 1-Fe complexes. One feature unique to the high-spin results are the large spin populations on the ligands, especially for the bridging sulfurs.

It is of special interest to compare the high-spin reduced 2-Fe model (Table IV) with the low-spin form of the oxidized 4-Fe cluster (Table III), since, from a spin-Hamiltonian point of view, the latter cluster may be considered as comprised of two of the former.[6,18] The comparison based on populations is not strong; the 2-Fe cluster has lower 3d populations and higher spin densities (especially for the sulfurs) than the 4-Fe complex. These differences probably reflect two ways in which the 4-Fe cluster is not like two 2-Fe clusters. First, the Fe–S^*_2–Fe unit is planar in the 2-Fe cluster but not in the 4-Fe. Second, the bridging sulfurs connect two parallel-spin iron atoms in the high-spin 2-Fe complex (and hence have a high-spin population, +0.45); in the 4-Fe cluster, S* bridges three iron atoms, one with spin opposite in direction to the other two (leading to a low-spin population, 0.06). The higher terminal S spin population in the 4-Fe cluster relative to the 2-Fe probably results from the fact that there is only one terminal S per iron atom in the larger complex, compared to two for the smaller cluster. In spite of these differences in overall charges, the orbital energy patterns are similar, as we saw above, so that many spectroscopic features of the high-spin reduced 2-Fe complex should resemble those of the oxidized 4-Fe complex.

Table V considers changes that occur when the various iron–sulfur clusters are reduced. Results for the 4-Fe cluster illustrate a common theme: even though the orbital accepting the extra electron ($9a_2$, see Table II) has about 90% iron character, reduction increases the population of the two more reduced irons by a total of only 0.14 electron. Small changes in the other orbitals distribute the remaining 0.86 electron among sulfur and methyl groups and the two more oxidized iron atoms. Although the iron population changes by only a small amount, the spin populations of the two more reduced iron atoms change by more, decreasing in absolute magnitude by a total of 0.42. This is the direction one would expect since the sixth d electron must be opposite in spin to the first five. There is a small *increase* (totalling 0.1 electron) in the spin populations of the more oxidized iron sites upon reduction, making them even more like the iron atom in the oxidized 1-Fe system.

The charge distribution in the 2-Fe cluster also displays some interesting features upon reduction. Here the change in iron charge is greater, especially for the 3d shell, where the increase is 0.22 for a single center (Table V). A significant fraction of the is in the Fe $3d_{z^2}$ orbital, which arises from occupying the mainly d_{z^2} $12a_1$ orbital (see Figure 3). We show below how this affects the Mössbauer quadrupole splitting at the reduced site. Upon reduction there are also increases in the electronic populations at all sulfurs, in the order S(red) ≈ S* > S(ox); here "ox" and "red" denote terminal sulfurs adjacent to the oxidized and reduced Fe sites. Such charge increases should lead to enhanced hydrogen bonding in the reduced forms in proteins where hydrogen donors are available (see section VII).

These changes parallel closely the corresponding changes on Fe, S*, and S when the 4-Fe cluster is reduced, indicating a close comparison between the electronic structures of the two types of cluster. As we discuss below, the changes that take place in the sulfur charge and spin distributions may plausibly be related to the mechanism for electron transfer and chemical reactions that are associated with these clusters.

Nature of the Iron–Sulfur Bonds

There are two principal groups of orbitals that contribute to the Fe–S σ bonds: the majority spin magnetic orbitals (which are mainly Fe 3d with some sulfur 3p character), and the minority spin S and S* orbitals, which delocalize to some extent onto the empty minority spin iron orbitals. The relative energies and characters of these orbitals suggests that the bridge S*–Fe bonding is stronger that the terminal S–Fe bonding, since the lower energy orbitals have more S*–Fe character (see Figures 3 and 4.)

For the 2-Fe clusters, the terminal S–Fe bond strength also depends upon the geometric orientation of the SR groups (R = H in the calculations, R = cysteine in proteins). This is illustrated in Figure 6 which shows the $8a_1\uparrow$ (majority spin magnetic) and $12a_1\uparrow$ (accepting orbital) for geometries C and D of the reduced 2-Fe model. The $8a_1$ orbital is typical of Fe–S bonding interactions, and changes in the S 3p orientation with geometry are due to the requirement to maintain orthogonality with the adjacent (and lower lying) S–H bond. As shown in the figure, the Fe 3d–S 3p overlap is more favorable in the upper part of the figure, where the hydrogens are pointed away from the Fe–Fe axis. Where known, the SR orientation in proteins is usually intermediate between the two idealized structures considered here.

Geometric factors also influence the shape of the mostly nonbonding orbital $12a_1$ (right side of Figure 6) which accepts the reducing electron in 2-Fe ferredoxins. As discussed earlier,[6] this orbital can be written as $\cos\theta\ (d_{z^2}) + \sin\theta\ (d_{x^2-y^2})$. The bond

Table V. Charge and Spin Population Changes upon Reduction[a]

	$Fe(SH)_4^{1-,2-}$	$Fe(SCH_3)_4^{1-,2-}$	$Fe_2S_2(SH)_4^{2-,3-}$	$Fe_4S_4(SCH_3)_4^{2-,3-}$
		A. Charges[b]		
Fe (3d)	+0.30	+0.31	+0.00 (+0.22)	+0.04 (+0.10)
Fe (total)	+0.32	+0.33	+0.05 (+0.11)	+0.02 (+0.07)
S*			+0.15	+0.10 (+0.08)
S	+0.15	+0.14	+0.08 (+0.18)	+0.10 (+0.13)
		B. Spins[c]		
Fe (3d)	−0.30	−0.31	+0.14* (+0.19)	+0.08* (+0.17)
Fe (total)	−0.32	−0.32	+0.13* (+0.25)	+0.05* (+0.21)
S*			+0.13	+0.11* (+0.02)
S	−0.14	−0.14	−0.03 (+0.12)	−0.12 (+0.21)

[a] Values given are individual-atom charge or spin populations for the reduced cluster minus those for the oxidized cluster. Where two values are shown, the first is for the more oxidized half of the cluster, and the value in parentheses is for the more reduced half. [b] For charge populations, a positive sign means an increase in the electron population upon reduction. [c] For sites where the absolute magnitude of the spin density has increased upon reduction, the spin population is followed by an asterisk; for a decrease, no asterisk.

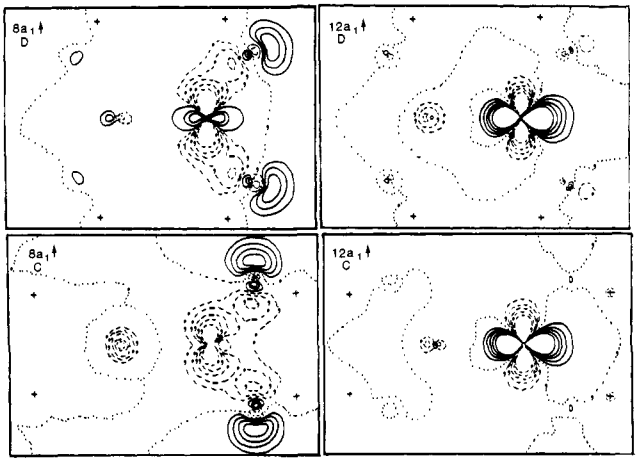

Figure 6. Contour diagrams for $Fe_2S_2(SH)_4^{2-}$. Left-hand side shows the $8a_1\uparrow$ Fe–S bonding orbital (see Figure 3); right-hand side shows the $12a_1\uparrow$ LUMO. Upper figures are for geometry D, lower figures for geometry C. The plane of the figure contains the 2Fe, 4S, and 4H atoms; locations of the hydrogens are marked by crosses. Contours (solid = positive, dashed = negative) are at ±0.005, ±0.075, ±0.10, ±0.125, and $\pm 0.16 a_0^{-3/2}$. Dotted contours are nodes.

strength relationship S*–Fe > S–Fe implies that θ is positive so that the $12a_1$ orbital has greater density along the y (in the terminal Fe–S plane) than along x (in the S* plane). In this way the orbital attains less antibonding character by avoiding the occupied electrons in the Fe–S* orbitals. As the SR orientation changes, the value of θ should decrease as the Fe–S bond becomes stronger, i.e., as the Fe–S and Fe–S* bonds become more nearly equal. This behavior is evident on the right side of Figure 6; although the differences in the $12a_1$ orbital are not large, we show below that such an effect should be observable in the Mössbauer quadrupole splittings.

It is also of interest to look at changes in iron–sulfur bond strength and covalency with cluster size. In assessing net bonding, three factors are important. (a) The low-lying Fe–S orbitals are bonding, with Fe–S* lower than Fe–S, as dicussed above. (b) More complex considerations arise when minority spin sulfur 3p electrons delocalize into the empty 3d orbitals of the adjacent iron atoms. The S* electrons can delocalize onto alternate sites with either spin-up or spin-down character, and hence are expected to be stabilized to a greater extent than the terminal S orbitals, which see only one adjacent iron atom. (c) The orientation of the terminal S 3p lone pairs is more constrained than the S* lone pairs, since the former must remain orthogonal to the S–R bonds.

The mean energy of S* 3p levels is below that of terminal S in both the 2-Fe and 4-Fe clusters, giving a relative bond strength Fe–S* > Fe–S. As Fe–S coordination is replaced by Fe–S* in the cluster sequence 1-Fe → 2-Fe → 4-Fe, there is an increase in Fe 3d population and a decrease in 3d and total spin population for equivalent oxidation states of Fe (Table III). The differences between the 1-Fe and 2-Fe complexes are greater than those between 2-Fe and 4-Fe.

Observed bond lengths for Fe–S* in 2-Fe complexes are shorter than the Fe–S bonds in either 1-Fe or 2-Fe complexes (see Table I), consistent with the bond strength estimates made above. The 4-Fe clusters have mean Fe–S* lengths similar to those for Fe–S, so that the difference between S and S* is less important. Similarly, the high-spin excited states of the $Fe_2S_2(SH)_4^{2-,3-}$ clusters are predicted to be more weakly bonded (and more ionic) than the low-spin forms, and to display larger Fe 3d spin populations and lower total Fe populations, i.e., to be more like the ionic Fe^{3+} structures.

Mössbauer Spectra

Mössbauer spectroscopy has been an important tool in unravelling the nature of charge and spin distributions in proteins and model complexes having iron–sulfur cores. For diamagnetic complexes, the spectra may yield two parameters, the isomer shift and the quadrupole splitting. For paramagnetic systems it is often also possible to determine the hyperfine interaction with the iron nucleus as well. Here we discuss theoretical predictions for these properties and compare them with experimental values.

Table VI. Mössbauer Isomer Shifts[a]

	$Fe(SH)_4$		$Fe_2S_2(SH)_4$		$Fe_4S_4(SCH_3)_4$	
	1–	2–	2–	3–	2–	3–
$\rho(0)$[b]	6.860	5.969	6.935	6.928, 5.944	6.023	5.780, 5.635
δ(calcd)[c]	0.23	0.51	0.20	0.20, 0.52	0.49	0.57, 0.62
δ(exptl)	0.25[d]	0.65[d]	0.26[f]	0.22, 0.56[d]	0.42[f]	0.50, 0.58[f]
(protein)				0.25, 0.54[g]		
δ(exptl)	0.13[e]	0.61[e]	0.17[f]		0.35[f]	0.57, 0.64[f]
(model)						

[a] Isomer shifts in mm/s, relative to metallic iron, at 4.2 K unless otherwise noted. Where two values are given, the first is for the more highly oxidized Fe, the second for the more highly reduced one. [b] Computed nonrelativistic charge density at Fe, minus $11870 a_0^{-3}$. [c] Determined from best-fit line of Figure 7. [d] Reference 22. [e] Reference 23. [f] Reference 15b and references therein. [g] Reference 12.

Isomer Shifts. The isomer shift is linearly related to the electronic charge density at the iron nucleus. The slope of the curve, however, is uncertain, since it depends upon the change in nuclear shape between the excited and ground states of the Mössbauer transition, for which accurate values are not known. Futhermore, relativistic effects are known to be important, but are not included in the present calculations. (For a general overview, see ref 19 and 20). Hence, we are led to consider semiempirical relations to estimate isomer shifts. Post and coworkers[21] have used results of Hartree–Fock calculations to develop the following relation between charge density at the nucleus ($\rho(0)$) and isomer shift:

$$\Delta I = (1.3)(-0.239 \text{ mm s}^{-1} a_0^3)\Delta\rho(0) \quad (1)$$

based on a linear plot of I vs. $\rho(0)$ for a number of Fe complexes. Here I is the isomer shift relative to Fe metal, and the factor of 1.3 is an approximate correction for relativistic effects. We show below that the slope given in eq 1 is in good agreement with the Xα results, but that the intercept of the I vs. $\rho(0)$ plot cannot be taken directly from the Hartree–Fock calculations since there is a substantial systematic difference in $\rho(0)$ between Xα and Hartree–Fock calculations.

A second, semiempirical, approach involves fitting a straight line by least squares to some or all of the Xα results, and using the resulting regression line as an interpolation formula. Table VI[22,23] presents results for isomer shifts for iron–sulfur clusters, and the data are plotted in Figure 7. We see that the linear relation between I and $\rho(0)$ is moderately good for the Fe–S clusters, but that some other iron complexes are not at all near the best-fit line. The least-squares line through the Fe–S data yields the relation:

$$I = 2.41 - 0.319(\rho(0) - 11870) \quad (2)$$

It is likely that the errors for the non-Fe–S clusters arise, at least in part, from the difficulty of comparing complexes of quite different coordination number and geometry. Within the Fe–S family, all of the iron atoms are tetrahedral and high spin, so that the approximations involved in the muffin-tin potential are about the same for all of them. It is clear from Figure 7 that we do not yet have the ability within the Xα scattered wave model to compare, for example, Fe–S isomer shifts with those of low-spin octahedral complexes such as ferricyanide. Hence, further work will be required a *general* procedure for making isomer shift calibrations from scattered wave results. The correlation within

(19) Shirley, D. A. *Rev. Mod. Phys.* **1964**, *36*, 339.
(20) Gutlich, P.; Link, R.; Trautwein, A. "Mossbauer Spectroscopy and Transition Metal Chemistry"; Springer-Verlag: New York, 1978, pp 60–84. Trautwein, A. *J. Phys. (Paris)* **1980**, *41*, C1–95.
(21) Post, D.; Van Duinen, P. Th.; Nieuwpoort, W. C. In ref 20, p 60.
(22) Thompson, C. L.; Johnson, C. E.; Dickson, C. P. E.; Cammack, R.; Hall, D. O.; Weber, U.; Rao, K. K. *Biochem. J.* **1974**, *139*, 97.
(23) Lane, R. W.; Ibers, J. A.; Frankel, R. B.; Papaefthymiou, G. C.; Holm, R. H. *J. Am. Chem. Soc.* **1977**, *99*, 84.

Table VII. Mössbauer Quadrupole Splittings[a]

theory			experiment
			A. $Fe(SH)_4^{1-,2-}$
ΔE_Q(ox) 1.05			0.57 (synthetic analogue,[b] 0.78 (rubredoxin)[c]
(red) −2.89			−3.28 (synthetic analogue), −3.16 (rubredoxin)[c]
			B. $Fe_2S_2(SH)_4^{2-}$
	A[i]	B[i]	
ΔE_Q	0.98	0.38	0.55 and 0.83 (algal),[d] 0.65 (spinach)[e], 0.61 (adrenal),[e] 0.36 (synthetic),[f] 0.60 (putida)[g]
η	0.57	0.73	0.5 ± 0.3, 0.5 ± 0.3, 0.5 ± 0.3, ---, 0.42
			C. $Fe_2S_2(SH)_4^{3-}$
	C[i]	D[i]	
Fe(ox) ΔE_Q	1.39	0.81	0.6 (algal),[d] 0.64 (spinach),[e] 0.81 (adrenal),[e] 0.6 (putida)[g]
η	0.42	0.77	0.3 ± 0.3, 0.6 (spinach), 0.5
Fe(red) ΔE_Q	+3.32	−3.11	−3.2 (algal),[d] −3.0 (spinach),[e] +2.7 (putida)[g]
η	0.69(x)	0.68(z)	0.0 ± 0.2(z), 0.0(z), 0.0(x)
$\lvert\theta\rvert$, deg	+24.4	+13.4	2 (algal),[h] 4 (spinach),[h] 17 (putida)[h]

[a] Quadrupole splittings are in mm/s. The nuclear quadrupole moment of ^{57}Fe is taken as 0.15 barn and the Sternheimer factor (1 - R) = 0.92 from ref 24. [b] Reference 23. [c] Reference 25. [d] Reference 26. [e] Reference 27 and 12. [f] Reference 28. [g] Reference 29. [h] Reference 30. [i] Geometry designation.

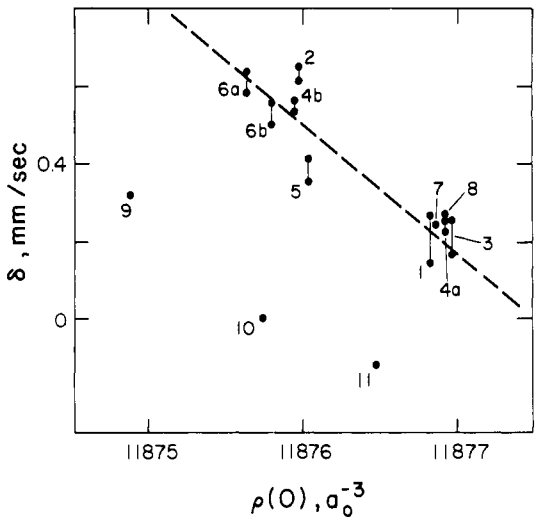

Figure 7. Plot of observed isomer shift vs. calculated nuclear charge densities. Key: (1) $Fe(SH)_4^-$; (2) $Fe(SH)_4^{2-}$; (3) $Fe_2S_2(SH)_4^{2-}$; (4) oxidized (a) and reduced (b) sites of $Fe_2S_2(SH)_4^{3-}$; (5) $Fe_4S_4(SCH_3)_4^{2-}$; (6) oxidized (a) and reduced (b) sites of $Fe_4S_4(SCH_3)_4^{3-}$; (7) Fe(Por)(Pyr)O_2 [Por = porphine, Pyr = pyridine]; (8) Fe(Por)(Pyr)CO; (9) $Fe(bpy)_3^{2+}$ [bpy = bipyridyl]; (10) $Fe(CN)_6^{3-}$; (11) $Fe(CN)_6^{4-}$. Observed values for (1) - (6) are collected in Table VI; two points connected by a line indicates a range of observed values, as given in Table VI. Computation details and observed values for (7) - (11) are given in ref 37 and 38.

the Fe–S group is good enough, however, to identify the interesting trends that we discuss next.

One of the surprising results from the charge distributions is that the Xα calculations indicate a higher Fe 3d population in the oxidized 2-Fe cluster (or at the Fe(ox) site of the reduced system) than in the corresponding 1-Fe model: 6.80 vs. 6.57 (see Table III). Other factors being equal, one expects this to lead to a larger isomer shift in the 2-Fe than in the corresponding 1-Fe cluster. However, both our isomer shift calculations and the experimental results for model complexes show only a small shift between the two clusters; in proteins, there is no shift to within experimental error. This emphasizes the fact that, even in clusters of nearly identical local geometry, the isomer shift, which depends upon the s orbitals, only indirectly reflects the 3d populations. Analyses based on Hartree–Fock calculations [20,21] have argued that the "potential distortion" effect caused by the Fe (3d) electrons is often of opposite sign to the "overlap distortion" effect caused by bonding effects in the molecular orbitals. Evidently these two contributions approximately cancel in this case, leading to no net isomer shift difference between the two clusters.

Table VI also shows that there is a smaller observed isomer shift in the oxidized 1-Fe and 2-Fe model complexes with substituents $(SR)_2$ = (S_2-o-Xyl) than in proteins where SR = cysteine. By electronegativity arguments, one expects (S_2-o-Xyl) to be more electron releasing than cysteine, resulting in a greater s density at Fe and a smaller isomer shift, in agreement with the observations. The SW calculations predict a substantially smaller isomer shift for R = CH_3 than for R = H in $Fe(SR)_4^-$: calculated values from eq 2 are 0.23 mm/s for R = H and 0.09 for R = CH_3. This shows that isomer shifts can be sensitive to changes in the second coordination shell around iron, so that comparisons between proteins and model complexes have to be made with some care.

Quadrupole Splittings. The Mössbauer quadrupole splittings (ΔE_Q) and asymmetry parameters (η) of Fe–S proteins depend on the following factors: (1) the basic electronic structure and oxidation state of the Fe–S core; (2) the geometric orientation and electronic structure of the cysteine residues; (3) the extent of electron donation or withdrawal by the rest of the protein. Table VII[24-30] gives predicted and experimental results, and it is clear that neither the theoretical calculations nor the synthetic models can account fully for the absolute values of the protein parameters. However, the Xα-SW theory does display a number of trends seen in the proteins.

We consider first the variation in predicted quadrupole splitting for different geometries. For $Fe_2S_2(SH)_4^{2-}$, the geometry change from A to B lowers the predicted quadrupole splitting. The experimental values (Table VII) span a range comparable to theory, with the synthetic model, $(SR)_2$ = (S_2-o-Xyl), at the low end and one site of algal ferredoxin at the high end. In the reduced 2-Fe theoretical models, the quadrupole splitting at the oxidized site similarly decreases upon changing geometry from C to D. Larger effects are observed at the reduced site. Here the calculated sign of the quadrupole splitting changes from positive to negative and the direction of the major axis from x to z (Table VII). The magnitude of the quadrupole splitting is large, about 3 mm/s, as is found experimentally. Note that spinach and putida ferredoxins differ in both the sign of the quadrupole splitting and in the direction of the major axis at the reduced site. This variation among proteins mimics differences in the calculations for geometries C and D.

(24) Lauer, S.; Marathe, V. R.; Trautwein, A. *Phys. Rev. A* **1979**, *19*, 1852.
(25) Phillips, W. D.; Poe, M.; Wieher, J. F.; McDonald, C. C.; Lovenberg, W. *Nature (London)* **1970**, *227*, 574.
(26) Anderson, R. E.; Dunham, W. R.; Sands, R. H.; Bearden, A. J.; Crespi, H. L. *Biochim. Biophys. Acta* **1975**, *408*, 306.
(27) Dunham, W. R.; Bearden, A. J.; Salmeen, I. T.; Palmer, G.; Sands, R. H.; Orme-Johnson, W. H.; Beinert, H. *Biochim. Biophys. Acta* **1971**, *253*, 134.
(28) Gillum, W. O.; Rankel, R. B.; Fouer, S.; Holm, R. H. *Inorg. Chem.* **1976**, *15*, 1095.
(29) Munck, E.; Debrunner, P. G.; Tsibris, J. C. M.; Gunsales, I. C. *Biochemistry* **1972**, *11*, 855.
(30) Bertrand, P.; Gayda, J. P. *Biochim. Biophys. Acta* **1979**, *579*, 107.

For the reduced 2-Fe clusters we have computed the amount of axial character in the orbital to which the reducing electron is added (i.e., $12a_1$ spin up; see Figures 3 and 6). As mentioned above, this orbital has the general form $\cos\theta\ (d_{z^2}) + \sin\theta\ (d_{x^2-y^2})$ on Fe(red). The value $\theta = 0°$ represents a pure axial d_{z^2} orbital. The transformation C → D reduces $|\theta|$, as well as changing the sign of the quadrupole splitting. This result is consisten with the fact that spinach and algal ferredoxins, with negative quadrupole splittings along z, have nearly axial LUMO's, $|\theta| = 4$ and 2°, respectively. Putida ferredoxin, on the other hand, has a positive quadrupole splitting and is far from axial. (The basis set Xα method also predicts a low value of θ, +8.1°, vs. +13.4° in the SW calculation, both for geometry D.[8]) Since the calculated Mössbauer results and θ values in geometry D are closer to those seen in typical ferredoxins, one might expect similar trends for other properties. We show elsewhere that, indeed, Zeeman and hyperfine tensors and d–d spectra in good agreement with experiment are predicted with geometry D and not with geometry C.[8]

At present, there are not enough experimental data to correlate systematically quadrupole splittings with geometry in most ferredoxins. The best situation exists for oxidized algal chloroplast ferredoxins, where the accurate Mössbauer spectra of Anderson et al.[26] for the species *Synechococcus lividus* can be compared with the X-ray structure at 2.5-Å resolution of the protein from *Spirulina platensis*.[31] (It has been established that the amino acid sequence of most chloroplast ferredoxins is invariant in the vicinity of the Fe–S core.) It appears from the X-ray structure that the two Fe sites are quite different in geometric structure, although both are distorted tetrahedra. This agrees with the observation of two quadrupole splittings in the oxidized protein, 0.55 and 0.83 mm/s. Neither Fe site has even approximate C_{2v} symmetry; the Fe–Cys 46, Cys 41 site has a approximate $C_2(z)$ axis and a geometry roughly intermediate between the theoretical C and D geometries; the Fe–Cys 79, Cys 49 site has a less regular geometry with Cys 79 roughly along z.

The good agreement of the theoretical Fe^{2+} quadrupole splitting in geometry D with the reduced Fe^{2+} splitting of algal ferredoxin probably means that the reduced site is Fe–Cys 46, Cys 41 and not Fe–Cys 79, Cys 49. In the latter case, it is unlikely that the added electron would be found in a d_{z^2}-type orbital; consequently, the major axis would not be z and ΔE_Q could have either sign. The Fe–Cys 46, Cys 41 site, however, should be geometrically compatible with a d_{z^2}-type LUMO.

The relationship between the electronic structure of 4-Fe complexes and their Mössbauer spectra can now be considered. For oxidized ferredoxin, our theoretical model predicts four iron sites with equivalent charge distributions, leading to a single quadrupole splitting and isomer shift. The delocalization of the sixth, minority spin 3d electron over two iron centers suggests that the observed parameters should be intermediate between the oxidized and reduced sites of 1-Feand 2-Fe complexes. Upon reduction, there are two inequivalent subsites in the 4-Fe clusters, with the iron atoms still equivalent in pairs. The extra electron should enter either the $9a_2$ or $14b_2$ orbitals (see Figure 4). The calculated energy splitting of these two orbitals is 0.12 eV in geometry F (Table II).

Table VIII shows results for both oxidized and reduced 4-Fe clusters. When $9a_2$ is occupied upon reduction, the orientation of the electric field gradient tensor is changed at the reduced iron site, but the overall quadrupole splitting is about the same as for the oxidized iron site. The alternative occupation of $14b_2$ yields a 1.2-mm/s difference in ΔE_Q between the reduced and oxidized sites, in qualitative agreement with the experimental observations.[15b,32-34] (The sign of ΔE_Q is not known experimentally.)

Table VIII. Mössbauer Quadrupole Splittings for 4-Fe Clusters[a]

cluster	ΔE_Q	η	ref
A. $Fe_4S_4(SCH_3)_4^{2-}$			
this work	−1.08	0.98	
exptl (synthetic)	1.10–1.26		32
exptl (HiPIP)	1.01		33
exptl (Fdox)	0.75		34
B. $Fe_4S_4(SCH_3)_4^{3-}$[b]			
this work, $9a_2$ occupied	1.36, 1.43	0.60, 0.59	
this work, $14b_2$ occupied	1.41, −2.63	0.60, 0.25	
exptl $Fe_4S_4(SPh)_4^{3-}$	1.13, 2.04[c]		15b
exptl $Fe_4S_4(SCH_2Ph)_4^{3-}$	0.93, 1.41		15b
exptl Fe(red)	1.32, 1.89		15b

[a] See footnote *a* to Table VII. [b] First value refers to the more highly oxidized Fe, second to the more highly reduced Fe. [c] Experimental values are for crystalline samples at 4.2 K.

The large variability in experimental values of ΔE_Q is consistent with the notion that the energy splitting between the $9a_2$ and $14b_2$ orbitals is a sensitive function of geometry. Spin–orbit mixing between these levels may also affect the quadrupole splittings; such considerations are beyond the scope of this paper. A more complete discussion of the Mössbauer spectra of the 4-Fe complexes will be presented elsewhere.

Discussion

In this section we summarize some of the important aspects of the electronic structure of Fe–S complexes, particularly with respect to physical and chemical properties and reactivity. We emphasize comparisons between different clusters as well as the effects of oxidation and spin state changes.

Nature of the Chemical Bonds. All of the clusters considered here may be viewed as containing high-spin monomer subunits (with $S = 2$ or $^5/_2$) that interact through ferromagnetic or antiferromagnetic interactions. The high degree of spin polarization on the iron atoms leads to an energy level ordering with the occupied Fe 3d levels well below the occupied S and S* 3p bands, and with the minority spin Fe 3d levels as the lowest unoccupied orbitals. This spin polarization also produces a splitting of the terminal S 3p levels, resulting in a spin population of S having the same sign as on the adjacent Fe. In terms of spin populations, the clusters are intermediate between the completely delocalized MO and the completely localized VB limits, being closer to the latter than the former.

Although these complexes have a highly ionic formal oxidation structures like $(SR)^-$–Fe^{3+}–$(S^*)^{2-}$, the bonding is better described as polar covalent, as judged by the near electroneutrality of the Fe and S populations (see Table III). In terms of simple resonance structures, radical configurations of the form $Fe^{2+}(d^6)$–(SR) and $Fe^{2+}(d^6)$–$(S^*)^-$ appear to make a larger contribution than the ionic structure in systems which formally contain Fe^{3+}. We also note that typical calculated Fe 4s + 4p populations are 1.2 electrons, rather than the zero value assumed in the idealized structures. The formally Fe^{3+} 3d populations are 6.6 to 6.8 electrons, with a nearly isotropic d electron distribution. Upon reduction, the 3d density becomes quite anisotropic, leading to large Mössbauer quadrupole splittings.

Interactions between Iron Sites. For both the 2-Fe and the 4-Fe cluster the orientations of the "spins" of the monomers may change upon excitation, creating "ladders" of states that can be approximated through a Heisenberg spin Hamiltonian. These excited electronic states lie within a few hundred wavenumbers of the ground state and many have significant thermal populations at room temperature. Our comparison of the high-spin and low-spin forms of the reduced 2-Fe complex indicates that the high spin form has a greater positive charge at Fe, and a more negative charge at S*, than does the low-spin form. More importantly, the high-spin form is expected to be a delocalized mixed-valence species, whereas the low-spin form is calculated (and observed)

(31) Tsukihara, T.; Fukuyama, K.; Nakamura, M.; Katsube, Y.; Tanaka, N.; Kakudo, M.; Wada, K.; Hase, T.; Matsubara, H. *J. Biochem.* **1981**, *90*, 1763.

(32) Holm, R. H.; Averill, B. A.; Herskovitz, T.; Frankel, R. B.; Gray, H. B.; Siiman, O.; Granthaner, F. J. *J. Am. Chem. Soc.* **1974**, *96*, 2644.

(33) Dickson, D. P. E.; Johnson, C. E.; Cammack, R.; Evans, M. C. W.; Hall, D. O.; Rao, K. K. *J. Biochem.* **1974**, *139*, 105.

(34) Thompson, C. L.; Johnson, C. E.; Dickson, D. P. E.; Cammack, R.; Hall, D. O.; Weser, U.; Rao, K. K. *J. Biochem.* **1974**, *139*, 97.

to have a trapped valence character. The reasons for this important difference between low-spin (antiferromagnetic) and high-spin (ferromagnetic) clusters have been discussed in some detail in ref 6.

Although 2-Fe ferredoxins appear to exist exclusively in the low-spin form, the possibility exists that geometric or environmental influences might favor a ferromagnetic interaction between the monomers in which the high-spin, delocalized form becomes the ground state. This appears to be the case for the oxidized 4-Fe clusters, for which the interaction energies between the 2-Fe subunits is apparently sufficient to drive each subunit into a high-spin conformation. Similar behavior has been postulated for certain 3-Fe clusters, which appear spectroscopically to be composed of a high-spin, reduced 2-Fe cluster coupled to the spin of a single Fe^{3+} unit.[35] An important area for future research will be to determine the circumstances favoring ferromagnetic vs. antiferromagnetic interactions in multinuclear clusters.

Electron Transfer. Upon reduction of all the "oxidized" clusters considered here, most of the added charge (56 to 70%) migrates to the sulfur atoms, as a result of changes in orbitals other than those which formally accept the extra electron. Both S and S* bear a negative charge, even in the oxidized complexes. These results are in accord with the extensive hydrogen bonding observed at both S and S* in iron-sulfur proteins, and with the increase in hydrogen bonding observed upon reduction of a 4-Fe "high-potential" Fe-S protein.[36]

The close proximity in energy of the filled S orbitals and empty Fe 3d orbitals (see Figures 2-4) may be important for the electron-transfer function of ferredoxins. In both 2-Fe and 4-Fe ferredoxins the iron sites are buried in the protein interior, whereas the cysteine sulfurs are more exposed to solvent. Internal electron transfer from cysteine S to Fe could be induced by the electrostatic field of a charged donor and might be the initial step in electron transfer; this would be followed by electron transfer from the donor to the more accessible hole in the S 3p band. In this context, it is of interest that the charge-transfer spectra of 2-Fe ferredoxins and their analogues begin at lower energy and have larger extinction coefficients than is the case for the 1-Fe rubredoxin. Indirect electron transfer of the type considered here should thus be a more facile process in the larger clusters.

The intimate relation between antiferromagnetic coupling and electron-transfer mechanism indicated above may also apply to other biological oxidation-reduction systems that have several metals, e.g., to cytochrome oxidase or nitrogenase. A common feature in all of these appears to be the presence of low-lying empty orbitals on the metal centers, in close proximity to filled orbitals on the ligands. A two-step electron-transfer model, such as that outlined above, could allow electrons to move over significant distances (10 Å or more) while still maintaining specificity at both the metal and the ligand sites. These characteristics are important for electron-transfer proteins and for multielectron oxido-reductases.

Acknowledgment. This research was supported in part by grants from the National Science Foundation (to J.G.N. and D.A.C.), the National Institutes of Health (to D.A.C.), the Petroleum Research Fund, administered by the American Chemical Society (to J.G.N.), and the DIB Office of the University of Chile (Project Q1759-8422 to A.A.). A.A. thanks SESI (Santiago) for providing computer time. L.N. is grateful for support from an NSF grant to Ernest R. Davidson during the writing of this manuscript. D.A.C. is an Alfred P. Sloan Foundation Fellow. We thank Michael Cook for helpful comments and for communicating details of his results prior to publication.

(35) Münck, E. In ref 1c, pp 147-175.
(36) Carter, C. W. Jr.; Kraut, J.; Freer, S. T.; Alden, R. A. *J. Biol. Chem.* **1974**, *249*, 6339. Adman, E. T.; Watenpaugh, K. D.; Jensen, L. H. *Proc. Natl. Acad. Sci. U.S.A.* **1975**, *72*, 4854.
(37) Aizman, A.; Case, D. A. *Inorg. Chem.* **1981**, *20*, 528.
(38) Case, D. A.; Huynh, B. H.; Karplus, M. *J. Am. Chem. Soc.* **1979**, *101*, 4433.

Properties of Some Protein Denaturants in *N,N*-Dimethylformamide. Enthalpic Interaction Coefficients of Urea and Substituted Urea Compounds

M. Bloemendal and G. Somsen*

Contribution from the Department of Chemistry, Free University, De Boelelaan 1083, 1081 HV Amsterdam, The Netherlands. *Received December 3, 1984*

Abstract: Enthalpies of dilution of urea and several alkyl-substituted ureas dissolved in *N,N*-dimethylformamide (DMF) have been measured calorimetrically at 298.15 K. The results are analyzed in terms of the McMillan-Mayer theory in order to obtain enthalpic interaction coefficients. For urea these coefficients are extraordinarily large. When an increasing number of methyl groups is introduced in the solute molecules, the values of the interaction coefficients change gradually to values usually found for compounds of this type. This is interpreted in terms of solute-solvent association. The enthalpic pair interaction coefficients of 1,1- and 1,3-dimethylurea differ distinctly. This indicates that simple additivity models are not applicable in this case. Considering DMF as a model system for the interior of a globular protein, the results are compared with those in water and discussed with respect to the denaturation of proteins by means of urea compounds.

This paper is part of a project in which we are investigating solute-solute interactions in nonaqueous solvents by means of enthalpic interaction coefficients on the basis of the McMillan-Mayer theory.[1] In this approach, which has been discussed by several authors,[2-6] the *n*th interaction coefficient refers to the interaction of *n* solute particles mediated by the solvent. In previous papers[6,7] we have reported results on several amides as solutes in the solvent *N,N*-dimethylformamide (DMF).

In this paper we focus our attention on urea and alkyl-substituted ureas. These compounds are of biochemical importance

(1) W. G. McMillan, Jr., and J. E. Mayer, *J. Chem. Phys.*, **13**, 276 (1945).
(2) H. L. Friedman, "Ionic Solution Theory", Interscience Publishers, New York, 1962.
(3) T. L. Hill, "An Introduction to Statistical Thermodynamics", Addison-Wesley Publishing Co., Reading, MA, 1962, Chapter 19.
(4) H. L. Friedman, *J. Solution Chem.*, **1**, 387, 413, 419 (1972).
(5) J. E. Desnoyers, G. Perron, L. Avédikian, and J.-P. Morel, *J. Solution Chem.*, **5**, 631 (1976).
(6) M. Bloemendal and G. Somsen, *J. Solution Chem.*, **12**, 83 (1983).
(7) M. Bloemendal and G. Somsen, *J. Solution Chem.*, **13**, 281 (1984).

0002-7863/85/1507-3426$01.50/0